The scintillation intensity and decay from Nd^{3+} $4f^2 5d$ and $4f^3$ excited states in several fluoride crystals

1993 J. Phys.: Condens. Matter 5 8437

(http://iopscience.iop.org/0953-8984/5/44/029)

J. Phys.: Condens. Matter 5 (1993) 8437–8460. Printed in the UK

The scintillation intensity and decay from Nd^{3+} $4f^25d$ and $4f^3$ excited states in several fluoride crystals

R Visser†, P Dorenbos†, C W E van Eijk†, A Meijerink‡ and H W den Hartog§

† Radiation Technology Group, Department of Applied Physics, Delft University of Technology, Mekelweg 15, 2629 JB Delft, The Netherlands

‡ Debye Research Institute, University of Utrecht, PO Box 80 000, 3508 TA Utrecht, The Netherlands

§ Solid State Physics Laboratory, State University of Groningen, Nijenborgh 18, 9747 AG Groningen, The Netherlands

Received 22 June 1993

Abstract. Nd^{3+}-doped LaF_3, $LiYF_4$, CsY_2F_7, BaY_2F_8 and BaF_2 crystals were investigated. For scintillator applications, the characteristics of the fast Nd^{3+} $4f^25d \rightarrow 4f^3$ emission component is of interest. The effective $4f^25d \rightarrow 4f^3$ scintillation decay time under gamma irradiation was found to vary from 5 to 42 ns, depending on the host lattice. Light yields were determined under x-ray excitation. The $4f^25d \rightarrow 4f^3$ output from many samples was seriously affected by impurity absorptions. After correcting for these, an estimate was made of the maximum possible $4f^25d \rightarrow 4f^3$ light yield to be expected in very pure Nd^{3+}-doped crystals. In neither of the cases was a $4f^25d \rightarrow 4f^3$ light yield of more than about 1000 photons per MeV of x-ray energy found. In addition to Nd^{3+} $4f^25d \rightarrow 4f^3$ emission, Nd^{3+} $4f^3 \rightarrow 4f^3$ and host emissions were also recorded at wavelengths shorter than 550 nm. A semi-quantitative model is given for the Nd^{3+} $4f^25d \rightarrow 4f^3$, $4f^3 \rightarrow 4f^3$ and host emission intensities.

1. Introduction

It has been shown by Yang and DeLuca [1,2] that Nd^{3+}, Er^{3+} or Tm^{3+} doping in several fluoride lattices gives rise to fluorescence in the vacuum ultra-violet (VUV) region, due to $4f^{n-1}5d \rightarrow 4f^n$ transitions in these ions. This observation was made under excitation by VUV photons or 10 keV electrons. Yang and DeLuca suggested the possibility of VUV lasing using these dopants. In LaF_3:Nd, optically pumped lasing has been shown by Waynant [3].

Because of its emission in the VUV region, LaF_3:Nd has also been considered as a scintillator for gamma-ray detection. In combination with a (VUV-sensitive) wire chamber, it may be used as a detector in positron emission tomography [4–6].

For the LaF_3:Nd crystal they studied, Gruwé and Tavernier [6] found an Nd^{3+} $4f^25d \rightarrow 4f^3$ light yield six times smaller than that of the short-wavelength (< 245 nm) cross-luminescence (CL) component of BaF_2, which is 1400 photons per MeV of absorbed gamma ray energy (photons MeV^{-1}) [7]. Hence, they concluded that LaF_3:Nd did not seem to be a promising scintillator material. However, in this work only one LaF_3:Nd crystal was investigated.

It can be expected that the scintillator performance depends on the Nd concentration and on the host lattice. In the present study we performed a systematic investigation of LaF_3, $LiYF_4$, CsY_2F_7, BaY_2F_8 and BaF_2 crystals doped with Nd^{3+} at many different concentrations.

0953-8984/93/448437+24$07.50

We studied the emission at wavelengths shorter than 550 nm, i.e. the wavelengths that can be detected by a bialkali photocathode. We observed emission originating from Nd^{3+} $4f^25d$ and $4f^3$ excited states and also different kinds of host emission: CL and self-trapped exciton (STE) emission. The present paper is concerned with describing the systematics of the emission intensities observed and with semi-quantitatively understanding them. Apart from the emission intensity, another important property, the decay of the scintillation, was also investigated.

2. Experimental methods

Neodymium-doped LaF_3, BaY_2F_8, and BaF_2 crystal boules were grown by one of us (HWdH) using the Bridgman technique in a gaseous He atmosphere. From the cylindrically shaped crystal boules , with a diameter of 7–8 mm, discs were cut and polished at the top and bottom faces. Several LaF_3 crystals containing more than 10 mol% Nd^{3+} were obtained from BDH-Crystan, Merck Ltd, Poole, UK. These crystals were also grown using the Bridgman technique. The Nd concentrations were calculated from the weighed-in amount of NdF_3. In some cases these calculated concentrations were not consistent with the measured absorption spectra. Then the concentration was determined by comparing the absorption spectra of samples consisting of the same host crystal but different Nd concentration.

On a first visual inspection, some of the LaF_3:Nd crystals were not clear, but (partly) opaque. Otherwise their appearance was good. The BaF_2:Nd crystals were all transparent. The BaY_2F_8:Nd crystal boules were largely polycrystalline, but small translucent samples could be obtained from the lower-doped boules. Useful measurements on the higher doped BaY_2F_8:Nd could only be done using very thin samples.

The $LiYF_4$ and CsY_2F_7 crystals were obtained from N M Khaidukov at the N S Kurnakov Institute of General And Inorganic Chemistry, Moscow, Russia. The $LiYF_4$ crystal was cut from a 22 mm diameter boule and was of good optical quality. CsY_2F_7 was grown using the hydrothermal synthesis technique. This yielded clear crystals of ~ 5 mm in diameter.

Optical absorption and emission spectra were measured using an ARC VM502 monochromator, an ARC 775 deuterium lamp or a W lamp and a Thorn EMI 9426 or Philips XP2020Q photomultiplier tube. High-energy excitation of the crystals was performed using an x-ray tube with a Cu anode, operated at 35 kV and 25 mA. The x-ray excited emission spectra were compared to those from pure BaF_2 samples, measured under identical experimental conditions. From this, and the known BaF_2 light yield of 1.1×10^4 photons MeV^{-1} [7, 8], light yields were determined. Optical decay measurements were performed with a Lambda Physik LPD-3002 dye laser pumped by an LPX-100 excimer laser. The experimental set-up has been described in detail in [9].

Scintillation decay measurements were performed using a ^{137}Cs gamma source, which emits 662 keV photons. This measurement is based on the single-photon-counting technique described by Bollinger and Thomas [10], and had a time resolution of 0.5 ns FWHM (full width at half maximum). As start and stop photomultipliers, two XP2020Q tubes were used, which are sensitive in the 160–600 nm wavelength region. All scintillation decay measurements were performed under identical geometry and electronics settings. All experimentally obtained data were corrected using the calibration curves for the equipment. As an exception, in the decay measurements, no correction was made for the wavelength dependence of the photomultiplier detection efficiency. Unless otherwise stated, all experiments were performed at room temperature.

3. Results

In section 3.1 the absorption spectra of some of our samples are presented. The x-ray-induced emission spectra from the same samples are given in section 3.2. Using the absorption and emission spectra we estimated the emission that would result from very pure Nd-doped LaF_3, $LiYF_4$, CsY_2F_7, BaY_2F_8 and BaF_2. The results from this absorption-correction procedure are presented in section 3.3. In section 3.4, using data from literature and from optical decay measurements (for BaF_2:Nd), we give an estimation of the quantum efficiencies of the Nd^{3+} $4f^25d \rightarrow 4f^3$ and $4f^3 \rightarrow 4f^3$ transitions in the different host materials. The quantum efficiency of a transition *upper state*→ *lower state* is defined as the probability that the upper state decays radiatively to the lower state. In section 3.5 results from the scintillation decay measurements are presented.

3.1. Optical absorption spectra

Figure 1 shows the absorption spectra of typical samples. At wavelengths longer than 240 nm the characteristic Nd^{3+} $4f^3 \rightarrow 4f^3$ absorption lines are observed [11]. The intense absorption at wavelengths shorter than 190 nm is due to Nd^{3+} $4f^3 \rightarrow 4f^25d$ transitions. The absorption edge shifts to longer wavelengths in the sequence LaF_3, $LiYF_4$, CsY_2F_7, BaY_2F_8, BaF_2.

The absorption spectra in figure 1 of the Nd-doped LaF_3 and BaF_2 crystals show impurity Pr^{3+} $4f^2 \rightarrow 4f5d$ absorption bands near 180 and 210 nm respectively [12, 13]. Beside Nd^{3+} and Pr^{3+} absorption, a gradual increase of the absorption towards shorter wavelengths is observed in most crystals. Such structureless absorption was reported before in LaF_3 crystals grown from not very well purified source material [14].

In absorption spectrum d, figure 1, of 0.45 mm thick BaY_2F_8:Nd (1.2 mol%), the bands at 157 and 178 nm are due to Nd^{3+} $4f^3 \rightarrow 4f^25d$ transitions [15]. In thicker and/or higher-doped samples, $4f^3 \rightarrow 4f^3$ absorptions were observed near 327 and 353 nm. The origin of the absorption bands at 169 and 192 nm is not clear. In any case these absorptions are not due to Pr^{3+} or Ce^{3+} impurities, since these ions absorb at other wavelengths [15]. An absorption structure, similar to the $\sim$ 192 nm band in BaY_2F_8 and also peaking about 14 nm above the highest-wavelength $4f^3 \rightarrow 4f^25d$ absorption band of Nd^{3+}, was observed in LaF_3:Nd samples of bad quality.

3.2. X-ray-induced emission spectra

Figure 2 shows the emission spectra, obtained from the samples of figure 1, under x-ray excitation. Except for the BaF_2:Nd sample shown, the spectra are dominated by Nd^{3+} emission. At wavelengths shorter than 300 nm, Nd^{3+} $4f^25d \rightarrow 4f^3$ emission is observed. We note the gradual increase of the peak wavelength of the Nd^{3+} $4f^25d \rightarrow 4f^3$ emission in the sequence LaF_3, $LiYF_4$, CsY_2F_7, BaY_2F_8, BaF_2. This is due to the shift of the $4f^25d$ states to lower energies, which was also observed in the absorption spectra.

At the low spectral resolution of figure 2, the $4f^25d \rightarrow 4f^3$ emission consists of three bands. The most intense band, which is located at the shortest wavelength, can be assigned to transitions from the lowest $4f^25d$ level to the $4f^3$ ^4I_J levels. The other two bands are assigned to transitions from the lowest $4f^25d$ level to the energy levels between the $4f^3$ $^4F_{3/2}$ and the lowest $4f^3$ $^2D_{5/2}$ levels [11]. The most intense band was also investigated at 1.5 nm wavelength resolution (FWHM). This experiment did not reveal significant additional fine structure for the samples shown in figure 2, with the exception of the $LiYF_4$:Nd (0.9 mol%) sample. The band near 180 nm was found to consist of two sub-bands, one centred

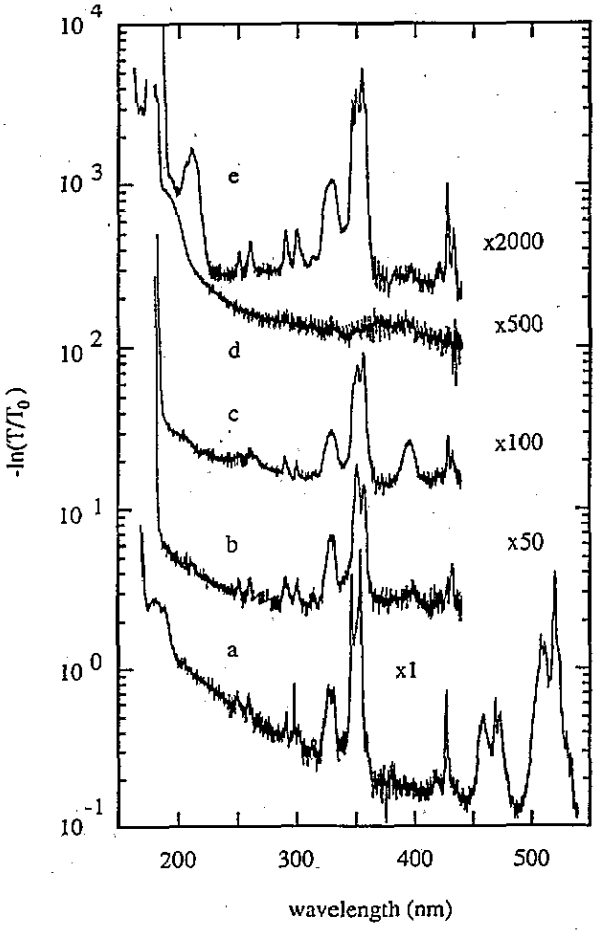

Figure 1. Optical absorption spectra for 2.0 mm thick LaF_3:Nd (13.8 mol%) (curve a), 7.0 mm thick $LiYF_4$:Nd (0.9 mol%) (curve b) 2.3 mm thick CsY_2F_7:Nd (3.0 mol%) (curve c), 0.45 mm thick BaY_2F_8:Nd (1.2 mol%) (curve d), and 2.2 mm thick BaF_2:Nd (11 mol%) (curve e). T_0 is approximately the maximal transmission observed, which is close to unity in clear samples. The spectral resolution is 1.5 nm (FWHM). For clarity, the spectra have been multiplied by the factors shown.

at 182 nm and another at 186 nm. The height of the former band was 1.3±0.2 times that of the latter one. These two peaks were also observed by Deviatkova *et al* [16] using optical excitation into the higher-energy Nd^{3+} $4f^3 \rightarrow 4f^25d$ absorption bands. The relative peak height was about 1.7, i.e. similar to the value we found. Only one peak was observed if the lowest $4f^3 \rightarrow 4f^25d$ transition was excited, using 176 nm light.

We did not study the $4f^3 \rightarrow 4f^3$ emission bands at a spectral resolution better than that shown in figure 2. More detailed spectra can be found in [17] for LaF_3, [18] for BaY_2F_8, and [19] and [20] for BaF_2.

Emission bands not arising from Nd^{3+} were also found. In LaF_3, Pr^{3+} emission bands at 251, 272 and 397 nm originating from the $^1S_0$ level are observed in the emission spectrum a in figure 2 [17, 12]. In the weakly doped LaF_3 crystals, we observed an appreciable amount of host luminescence. This is shown in figure 3. Brixner *et al* [21] assigned this host emission band to V_K–e recombination. We will call this host emission STE emission. At room temperature, the STE emission is considerably thermally quenched, which is evident from figure 3.

Host emission was also found in BaY_2F_8. After correcting for the absorption by the sample itself, we found a broad structureless band peaking at about 250 nm, having half the peak intensity at about 160 and 360 nm, and one tenth the peak intensity at 500 nm.

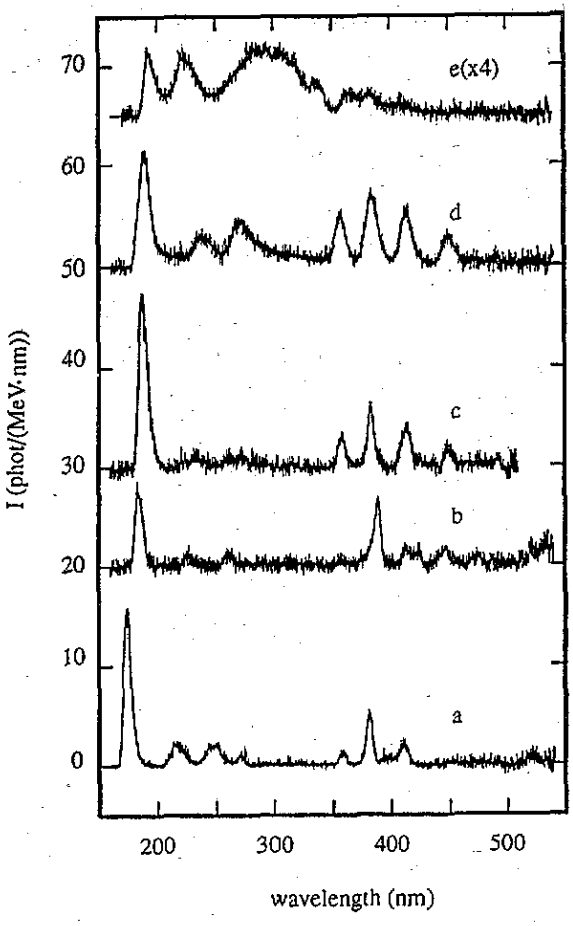

Figure 2. X-ray-induced emission spectra (*not* absorption corrected) of 2.0 mm thick LaF_3:Nd (13.8 mol%) (curve a), 7.0 mm thick $LiYF_4$:Nd (0.9 mol%) (curve b), 2.3 mm thick CsY_2F_7:Nd (3.0 mol%) (curve c), 0.45 mm thick BaY_2F_8:Nd (1.2 mol%) (curve d), and 2.2 mm thick BaF_2:Nd (11 mol%) (curve e). The spectral resolution is about 6 nm (FWHM). For clarity, the spectra a, b, c, d and e have been shifted by 0, 20, 30, 50 and 65 photons MeV^{-1} nm^{-1}), respectively.

These values are only accurate within an error of about 40 nm. The part extending from 4 to 7.5 eV has been reported on before and ascribed to CL emission [22].

In BaF_2, host emission dominates the emission spectrum. Figure 2, spectrum e, clearly shows the presence of the CL bands near 195 and 220 nm and the broad STE emission band centred near 300 nm [39]. Very weak Nd^{3+} $4f^25d \rightarrow 4f^3$ and Nd^{3+} $4f^3 \rightarrow 4f^3$ emission is present in the spectra. The emission at 192 nm in the 11 mol% doped sample is more intense than expected if only CL were present, which indicates that the main Nd^{3+} $4f^25d \rightarrow 4f^3$ emission peak is located in this wavelength region. Weak $4f^3 \rightarrow 4f^3$ bands at 382 and 412 nm can also be observed.

3.3. Absorption-corrected x-ray-induced light output

The optical absorption of many samples greatly influenced the emission intensity. For a large part, the optical absorption is due to unwanted impurities, especially in the short-wavelength range. We are interested in the number of photons emitted in the samples, before absorption by the sample itself. This quantity is obtained by correcting the emission spectra for the absorptions. Generally, at about 400 nm no correction was necessary. At this wavelength, in clear samples the measured transmission was $2n/(n^2+1)$ within error. Here n is the refractive index (at 400 nm). The quotient is the theoretically expected

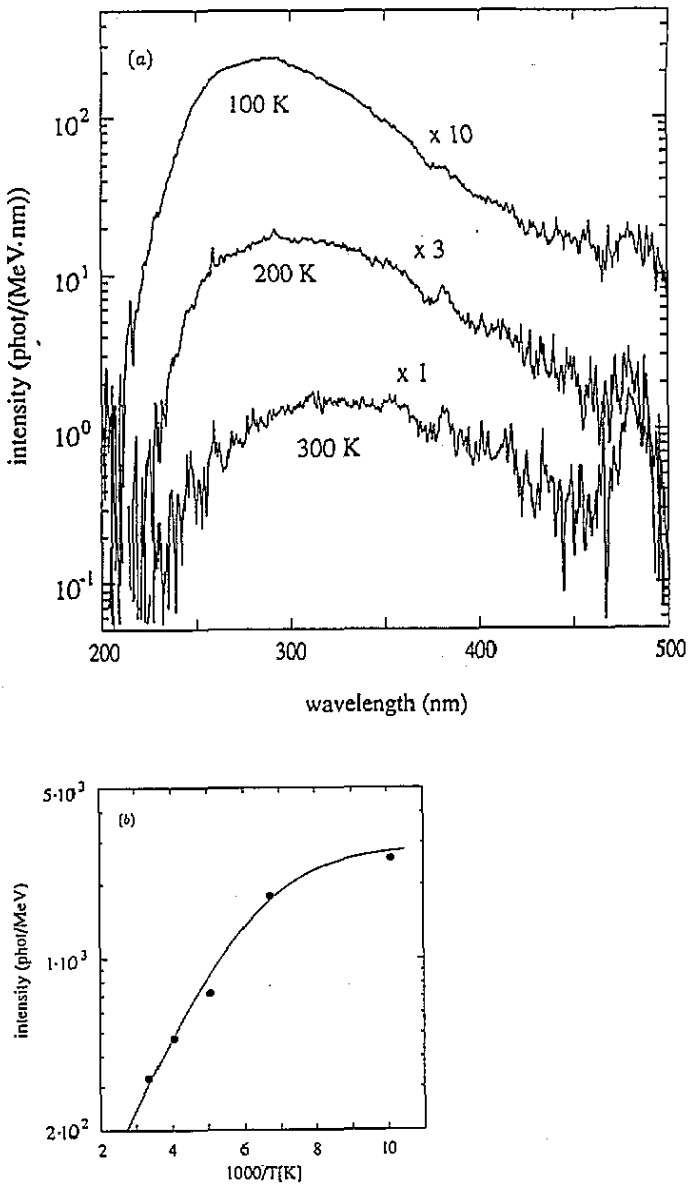

Figure 3. (*a*) Emission spectra for a nominally pure 0.45 mm thick LaF_3 sample, recorded at different temperatures. Beside host emission, weak impurity bands are visible due to Nd^{3+}. The spectral resolution is 4 nm (FWHM). (*b*) The temperature dependence of the total light output. The theoretical fit is discussed in the text (16).

transmission if the transmission of the bulk of the crystal is unity and only some incoming light is reflected at the (parallel) crystal surfaces. At shorter wavelengths, this transmission decreases somewhat, because n increases. For instance, in LaF_3 $2n/(n^2+1) = 0.91$ at 2.0 μm and 0.87 at 0.2 μm [23]. This effect is not large enough to explain the observed gradual decrease of the transmission towards shorter wavelengths. This is indicative for impurity absorptions at short wavelengths.

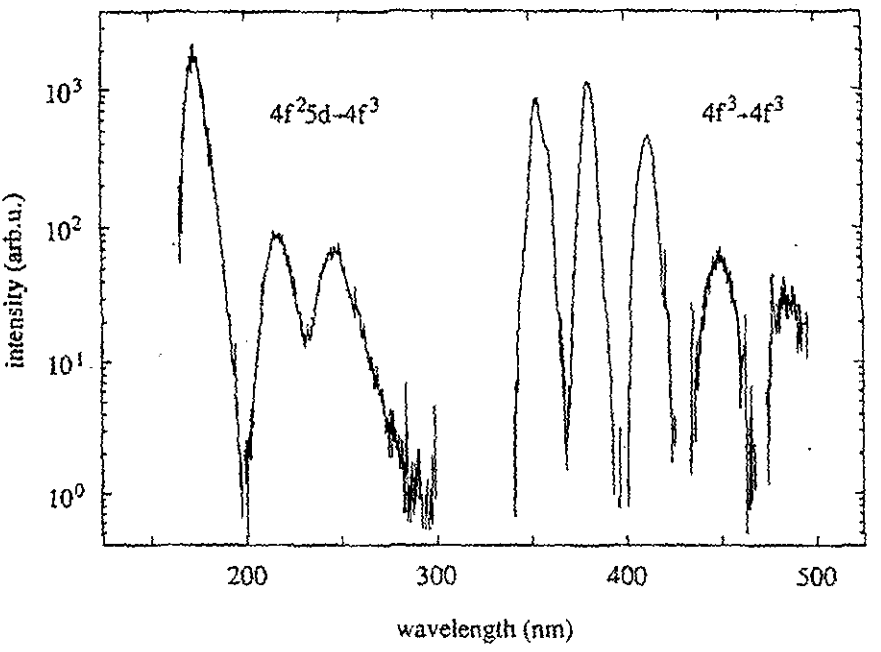

Figure 4. Absorption-corrected Nd^{3+} $4f^25d \rightarrow 4f^3$ and $4f^3 \rightarrow 4f^3$ emission bands in LaF_3. The spectral resolution is 4 nm (FWHM).

The optical path length through the crystal covered by photons from the lamp in an absorption measurement or from the thin emitting surface layer of the crystal in an x-ray-excited emission measurement are about the same. The reason for this is that in the emission measurements, the sample was placed in between the x-ray tube and the entrance slits of the monochromator, such that only photons emitted at right angles to the crystal surface were detected. The same arrangement was used in the absorption measurements, but now the x-ray tube was replaced with a lamp. From this and the preceding paragraph, it follows that the number of photons created in the crystal, i.e. the absorption-corrected emission spectrum, is simply the measured emission spectrum divided by the measured transmission spectrum and multiplied by the measured transmission at 400 nm. Here a small error is made because the factor $2n/(n^2+1)$, which is wavelength dependent, is replaced with a fixed value (at 400 nm). This was done because the refractive index was not known for each crystal at all wavelengths.

Some samples were not clear, but polycrystalline or opaque. This may be due to O contamination, as was pointed out by Korczak and Mikolajczak [24]. This caused scattering of incident light, resulting in a lower measured transmission at all wavelengths. The measured emission intensity is not very much affected by scattering of light in the crystal, because the light is emitted in all directions. Therefore, for these crystals also the above absorption correction is reasonable, since correction is necessary only for the bulk absorption, and not for the scattering. The bulk absorption is described by the measured transmission spectrum, divided by the transmission at 400 nm.

In general, the absorption-corrected emission spectra could be decomposed into a limited number of bands. The absorption-corrected Nd^{3+} $4f^25d \rightarrow 4f^3$ and $4f^3 \rightarrow 4f^3$ emission bands obtained for LaF_3 are shown in figure 4. The absorption-corrected STE emission band

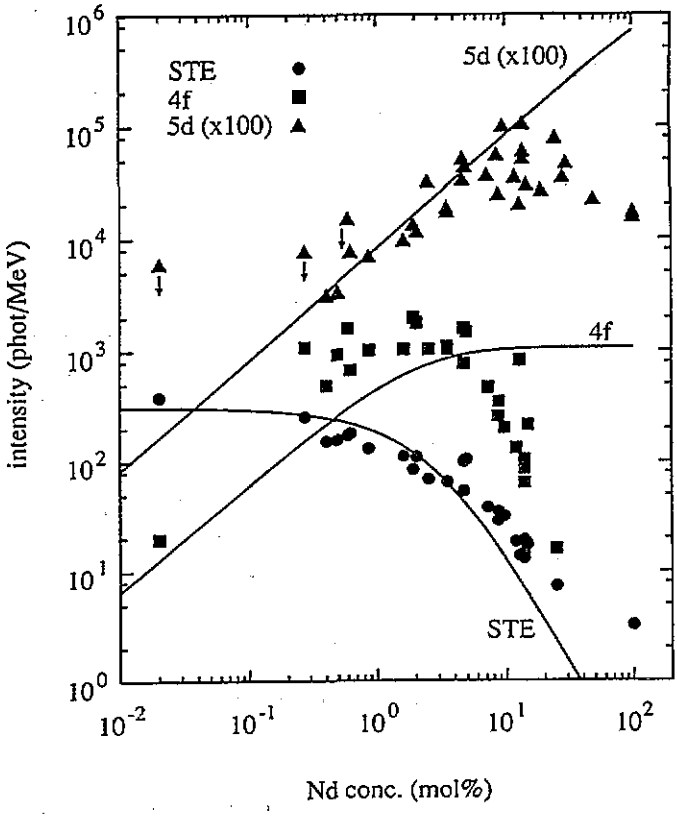

Figure 5. Absorption-corrected emission intensities from $LaF_3:Nd^{3+}$ crystals. The x-ray-induced intensities for wavelengths < 550 nm of the Nd^{3+} $4f^25d \rightarrow 4f^3$ bands (*5d*) and of the $4f^3 \rightarrow 4f^3$ bands (4f), and of the LaF_3 host emission (STE) are shown. Downward pointing arrows mean that the intensity may be lower than indicated. The 0.02 mol% data pertain to a $\leqslant 0.02$ mol% doped sample. The curves were calculated using (19) (*5d*) or (9)–(13) and the LaF_3 data in table 4 for $s = 6$ (STE and 4f). For $s = 8$, very similar STE and 4f curves were obtained. All *5d* data were multiplied by 100 for clarity.

is similar to the broad bands shown in figure 3(*a*): it is a structureless band peaking at 300 nm with half the peak intensity at 250 and 370 nm (the accuracy of these values is 10 nm). For each Nd concentration, the LaF_3:Nd emission spectra could be described as a weighted sum of the Nd^{3+} $4f^25d \rightarrow 4f^3$, Nd^{3+} $4f^3 \rightarrow 4f^3$ and STE emission bands. Such a decomposition of the emission spectra into Nd^{3+} $4f^25d \rightarrow 4f^3$, Nd^{3+} $4f^3 \rightarrow 4f^3$, and host emission bands was performed for each of the host lattices. Minor emission components from unwanted trace impurities (e.g. Pr^{3+} or other rare earth ions) were neglected. Once the above weighted sums were established, the wavelength-integrated light yield due to each type of emission band could be determined. The results are shown in figure 5 for LaF_3, in figure 6 for $LiYF_4$, CsY_2F_7 and BaY_2F_8 and in figure 7 for BaF_2.

In the Nd^{3+}-doped $LiYF_4$ and CsY_2F_7 samples, we did not observe host emission. However, in a pure CsY_2F_7 crystal an STE-like emission band has been observed. The maximum is located at about 300 nm and the width of the band is about 150 nm (FWHM). Its intensity is 100±20 photons MeV^{-1} at 294 K and 1000±200 photons MeV^{-1} at 100 K.

The (absorption-corrected) emission intensity of the BaY_2F_8 host luminescence was

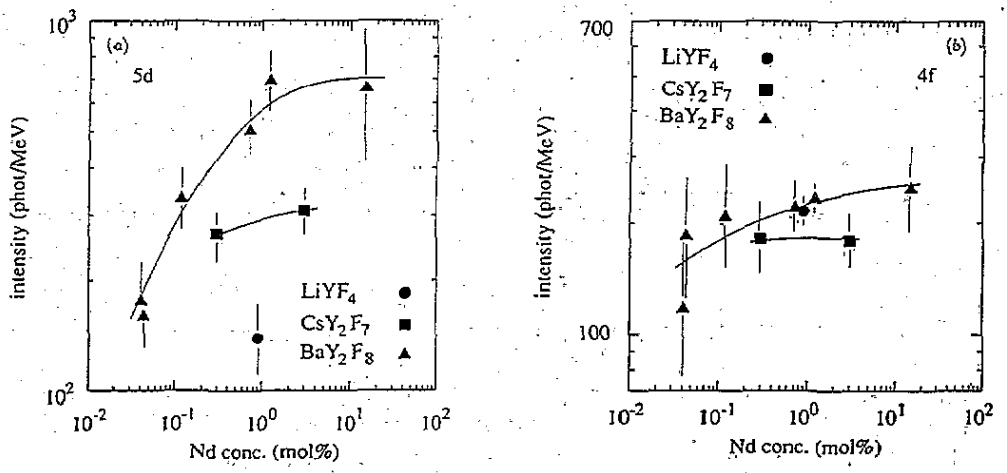

Figure 6. X-ray induced intensity of the Nd^{3+} $4f^25d \rightarrow 4f^3$ (*a*) and Nd^{3+} $4f^3 \rightarrow 4f^3$ (*b*) absorption-corrected emission bands (for $\lambda < 550$ nm) from Nd^{3+}-doped $LiYF_4$, CsY_2F_7 and BaY_2F_8. The curves are merely guides to the eye.

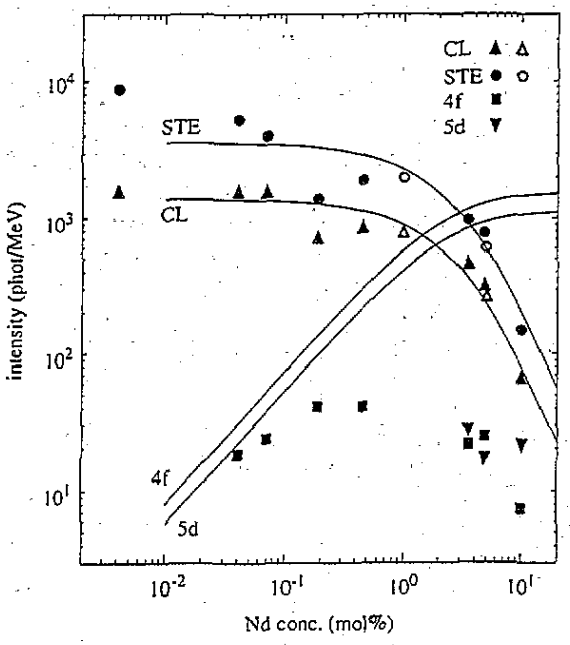

Figure 7. X-ray induced emission intensities of the CL, STE, Nd^{3+} $4f^3 \rightarrow 4f^3$ and Nd^{3+} $4f^25d \rightarrow 4f^3$ bands in BaF_2:Nd (respectively denoted CL, STE, 4f and 5d in the figure). The data points at 4×10^{-3} mol% pertain to a nominally undoped BaF_2 sample. The open CL and STE data points are from [25], normalized to the intensities CL= 1400 and STE= 9500 photons MeV^{-1} in the undoped BaF_2 [7]. The curves were calculated using (9)–(13) and the BaF_2 CL and STE data for $s = 6$ in table 4.

500±100 photons MeV^{-1} at Nd concentrations up to 1 mol%. For higher Nd concentrations, the light yield decreases. In the 15 mol% doped sample less than 200 photons MeV^{-1} remain.

3.4. Estimation of the Nd^{3+} quantum efficiencies

We did not directly measure the quantum efficiencies of the Nd^{3+} ion in the distinct host lattices. Instead, we used decay-time data from the literature or from optical excitation experiments (for BaF_2) in order to obtain a rough estimate for the non-radiative decay from

Table 1. Decay times in microseconds of the Nd^{3+} $4f^3$ $^4D_{3/2}$ and $^2P_{3/2}$ excited states. LaF_3, $LiYF_4$ and BaY_2F_8 data are from literature; BaF_2 data are from this work. The experimental errors in most data are a few per cent.

Host	LaF_3 [49,27] 0.1 mol% Nd			$LiYF_4$ [27] 0.1 mol%		BaY_2F_8 [18] 0.4mol% Nd			BaF_2 0.07 mol% Nd		
	6 K	77 K	300 K	6 K	300 K	6 K	60 K	300 K	4 K	66 K	300K
$\tau(^4D_{3/2})$	42	34.6	22.7 13.5	1.3	1.3	4.2	4.5	2.7	42	58	14
$\tau(^2P_{3/2})$	421	400.5	212.7 225	50	35	116	116	50	1040	1107	232

the Nd^{3+} $4f^25d$, $4f^3$ $^4D_{3/2}$ and $4f^3$ $^2P_{3/2}$ levels. The $4f^25d \rightarrow 4f^3$ and $4f^3 \rightarrow 4f^3$ emission bands we observed are due to transitions from these levels to lower Nd^{3+} levels. Below we successively discuss the $4f^25d \rightarrow 4f^3$ and $4f^3 \rightarrow 4f^3$ quantum efficiencies.

3.4.1. $4f^25d \rightarrow 4f^3$ quantum efficiency. Yang and DeLuca [1,2] have found that the quantum efficiency of transitions from the lowest Nd^{3+} $4f^25d$ state in 0.1 mol% doped YF_3 and LuF_3 is about 0.8. This high quantum efficiency is in agreement with the fact that they did not observe emission around 388 nm (due to transitions within the $4f^3$ configuration) when optically exciting the Nd^{3+} ions into the $4f^25d$ states. For 0.5 mol% doped LaF_3 and $LiYF_4$, the $4f^3 \rightarrow 4f^25d$ related bands in the excitation spectrum of the 388 nm emission were also very weak. This suggests that in these host lattices, the $4f^25d \rightarrow 4f^3$ quantum efficiency may be high too.

In CsY_2F_7, BaY_2F_8 and BaF_2, the Nd^{3+} $4f^25d \rightarrow 4f^3$ quantum efficiency may be lower, since in these host lattices the Nd^{3+} $4f^25d$ states lie about 650–1600 cm^{-1} lower than in $LiYF_4$: the $4f^3 \rightarrow 4f^25d$ absorption and emission structures are at longer wavelengths. Since the $4f^3$ energy levels are the same within a few 100 cm^{-1}, this means that the energy gap between the lowest $4f^25d$ and the next lower $4f^3$ level in these three crystals is smaller than that in LaF_3. Because the phonon frequencies involved are the same as or larger than those in LaF_3 [26], multi-phonon radiationless decay is probably more important than in LaF_3.

3.4.2. $4f^3 \rightarrow 4f^3$ quantum efficiency. The emission observed between 300 and 550 nm is due to radiative decay from the Nd^{3+} $4f^3$ $^4D_{3/2}$ and $^2P_{3/2}$ levels. The quantum efficiencies of transitions from these levels to lower $4f^3$ levels were estimated using the decay time data given in table 1. For the decay time τ we can write

$$1/\tau = 1/\tau_r + W \tag{1}$$

where $1/\tau_r$ is the radiative decay rate and W is the non-radiative decay rate. In general, the decay rate V from a Stark multiplet (V is $1/\tau_r$ or W) is determined by the thermal population of the Stark levels:

$$V = \sum_i V_i \, P_i(T) \qquad P_i(T) \equiv g_i \exp\frac{-\Delta_i}{kT} \Big/ \sum_i g_i \exp\frac{-\Delta_i}{kT} \tag{2}$$

where V_i are the individual decay rates for each Stark level (i.e. $1/\tau_{r,i}$ or W_i), g_i is the degeneracy and Δ_i is the energy separation from the bottom level [28]. The $^4D_{3/2}$ and $^2P_{3/2}$ Stark multiplets both consist of two levels of degeneracy $g_1 = g_2 = 2$. In LaF_3, Δ_i are 30–50 cm^{-1} and in $LiYF_4$ they about 100 cm^{-1} [11].

Table 2. A rough estimate of the Nd^{3+} $4f^3 \rightarrow 4f^3$ quantum efficiencies η for decay from the $4f^3$ $^4D_{3/2}$ and $^2P_{3/2}$ states. For the meaning of ΔE, $W^{(1)}(0)$ and $W^{(2)}(0)$, see the text. The errors in $W^{(1)}(0)$ were estimated from the scatter of the data points in the references cited.

Host		LaF_3 0.1 mol% Nd	$LiYF_4$ 0.1 mol% Nd	BaY_2F_8 0.4 mol% Nd	BaF_2 0.07 mol% Nd	
ΔE (cm^{-1}) [a]	$^4D_{3/2}$	1915 [11]	1752 [11]	1746 [18]	1935±10	
	$^2P_{3/2}$	2298 [11]	2239 [11]	2403 [18]	2270±50	
$1/W^{(1)}(0)$ (μs)	$^4D_{3/2}$	$70 \cdot 10^{\pm 0.1}$ [28]	$8 \cdot 10^{\pm 0.4}$ [31, 26]	—	$37 \cdot 10^{\pm 0.5}$ [30]	
	$^2P_{3/2}$	$550 \cdot 10^{\pm 0.1}$ [28]	$54 \cdot 10^{\pm 0.4}$ [31, 26]	—	$920 \cdot 10^{\pm 0.5}$ [30]	
$\hbar\omega$ (cm^{-1}) [26]		360	490	370	360	275
$1/W^{(2)}(0)$ (μs)	$^4D_{3/2}$	58±30[b]	$\geqslant 15$	9	34	146
	$^2P_{3/2}$	1136±60[b]	68	206	715	3531
η(300 K)	$^4D_{3/2}$	0.12	$\geqslant 0.91$	0.31	< 0	0.14
	$^2P_{3/2}$	0.33	0.18	0.19	< 0	0.14

[a] LaF_3, $LiYF_4$ and BaY_2F_8, $T \leqslant 10$ K; BaF_2 (this work), $T = 294$ K. In general, the temperature dependence is not large (e.g. LaF_3 $^4D_{3/2}$ at 77 K, 1936 cm^{-1} [11]).

[b] Error due to uncertainty in τ(300 K) (cf. table 1).

The non-radiative decay rates W_i can be due to multi-phonon decay within one Nd^{3+} ion or to energy transfer to neighbouring Nd^{3+} ions or other impurities present in the crystal. At low doping concentrations multi-phonon decay will dominate. Since for $4f^3$ levels electron–phonon interaction is weak, W_i can be written as [28]

$$W_i = W_i(0)\ (\bar{n} + 1)^p \qquad \bar{n} = 1/[\exp(\hbar\omega/kT) - 1] \qquad p = \Delta E/\hbar\omega. \tag{3}$$

This is an approximation of a more detailed expression for small values of the coupling parameter $L_m g_m^2$ [29]. $\bar{n}$ is the average number of phonons with energy $\hbar\omega$, $\hbar\omega$ being the effective energy of the phonons involved in the multi-phonon decay process. ΔE is the energy gap between the lowest Stark level of the multiplet considered and the first lower level. p is the effective order of the phonon emission process (we will also allow fractional values). For a given host material the constant $W_i(0)$ can be expressed within about an order of magnitude by

$$W_i(0) \simeq A \exp(-\alpha\, \Delta E) \tag{4}$$

where A and α depend on the host crystal and are about the same for each rare-earth-ion energy level [28, 30, 31].

We made an estimate of the quantum efficiency η. For this, we estimated the non-radiative decay rate W. We assumed that $P_i(T)$ can be approximated by a constant. Especially if the level splitting Δ_2 is not large and the temperature is not too low this is a reasonable approximation (see (2)). We write

$$W = W(0)\,(\bar{n} + 1)^p \tag{5}$$

where $W(0)$ is the effective average of $W_i(0)$. $W(0)$ was estimated in two ways. First, we estimated $W(0)$ according to (4), using the A and α parameters best fitting the experimental data [26, 28, 30, 31]. The result is denoted $W^{(1)}(0)$ in table 2. Second, $W(0)$ was estimated using the $\hbar\omega$ values proposed by Sveshnikova *et al* [26] and using the decay times in table 1. The result, $W^{(2)}(0)$, is obtained from the equation

$$W^{(2)}(0) = \left\{[\tau(300\ \mathrm{K})]^{-1} - [\tau(T_{\max})]^{-1}\right\} / \left\{\left[\bar{n}(300\ \mathrm{K}) + 1\right]^{\Delta E/\hbar\omega} - \left[\bar{n}(T_{\max}) + 1\right]^{\Delta E/\hbar\omega}\right\} \tag{6}$$

where $T_{\max}$ is the temperature at which the decay times in table 1 are maximal (e.g. for BaF_2, $T_{\max} = 66$ K).

In table 2 we observe reasonable coincidence between $W^{(1)}(0)$ and $W^{(2)}(0)$. The efficiency η at room temperature was determined from

$$\eta(300\ \mathrm{K}) = \tau(300\ \mathrm{K})/\tau_r \qquad 1/\tau_r = 1/\tau(T_{max}) - W^{(2)}(0)\,[\bar{n}(T_{max}) + 1]^{\Delta E/\hbar\omega} \tag{7}$$

where τ_r is the estimated radiative decay time. A special case is observed for BaF_2. Here the estimated non-radiative decay times $1/W(0)$ are shorter than the total decay times τ (cf. tables 1 and 2). In other words, τ_r is negative, which is clearly not physically correct. If we assumed a smaller value for $\hbar\omega$ this could be avoided. The smallest value which still yielded a reasonable fit to the decay-time data, see figure 8, is $\hbar\omega = 275\ \mathrm{cm}^{-1}$. The efficiencies obtained using this value are included in table 2.

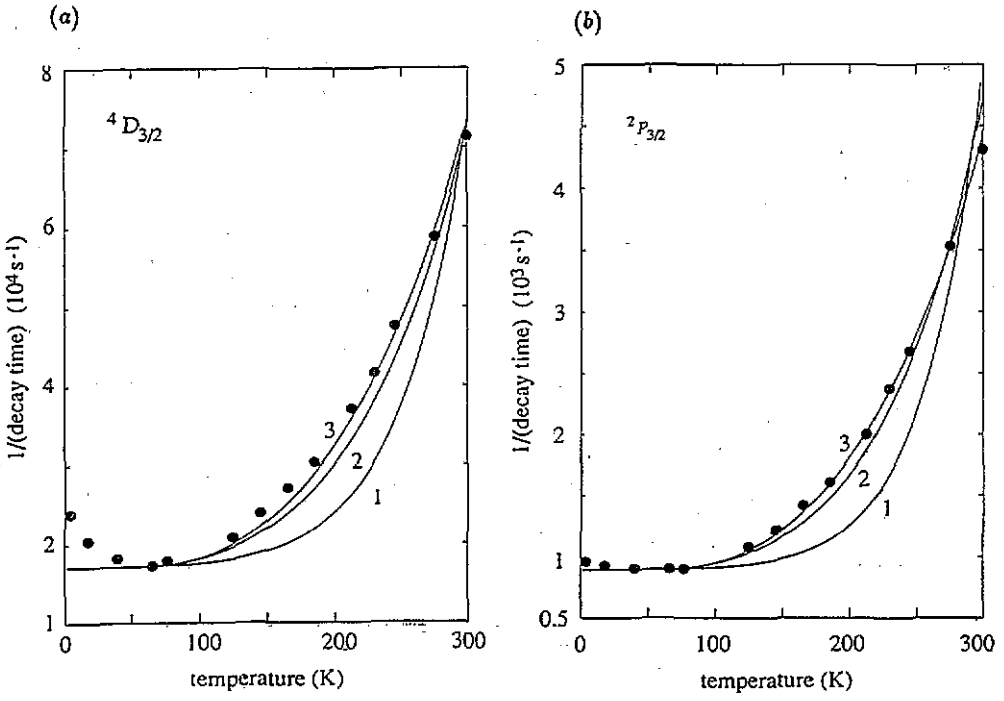

Figure 8. Experimental decay times (the data points) for the $^4D_{3/2}$ and $^2P_{3/2}$ levels obtained by optically exciting a BaF_2:Nd (0.07 mol%) sample at 342 nm and recording the emission at 383 nm ($^4D_{3/2} \rightarrow {}^4I_{11/2}$ transition) and 414 nm ($^2P_{3/2} \rightarrow {}^4I_{11/2}$ transition). (*a*) The decay rate $1/\tau(T)$ from the Nd^{3+} $4f^3$ $^4D_{3/2}$ multiplet. The curves were calculated using the relation $1/\tau(T) = (1/\tau_r) + W(0)\,(\bar{n}+1)^p$ (cf. (3)). The parameters $\hbar\omega$, $W(0)$ and $1/\tau_r$ are 200 cm^{-1}, 530 s^{-1}, 16 632 s^{-1} (curve 1); 275 cm^{-1}, 7000 s^{-1}, 10 101 s^{-1} (curve 2) and 325 cm^{-1}, 18340 s^{-1}, $-1193\ \mathrm{s}^{-1}$ (curve 3). The energy gap is $\Delta E = 1935\ \mathrm{cm}^{-1}$. (*b*) As (*a*), but for the $^2P_{3/2}$ multiplet. The parameters $\hbar\omega$, $W(0)$ and $1/\tau_r$ are 200 cm^{-1}, 17 s^{-1}, 883 s^{-1} (curve 1); 275 cm^{-1}, 320 s^{-1}, 575 s^{-1} (curve 2) and 350 cm^{-1}, 1250 s^{-1}, $-350\ \mathrm{s}^{-1}$ (curve 3). The energy gap is $\Delta E = 2270\ \mathrm{cm}^{-1}$.

3.5. Decay of the gamma-induced emission

Using 662 keV gamma rays from a ^{137}Cs source, we investigated the scintillation decay. We have isolated the $4f^25d \rightarrow 4f^3$ emission from LaF_3:Nd by performing one measurement in

N_2 atmosphere (short wavelength cut-off at 160 nm) and one in air (short-wavelength cut-off at 180 nm). Subsequently, the two measurements were subtracted. The $4f^25d \rightarrow 4f^3$ emission in other crystals was isolated by performing one measurement in air and another also in air, but using a UV filter (short wavelength cut-off at 280 nm) between the sample and the detector.

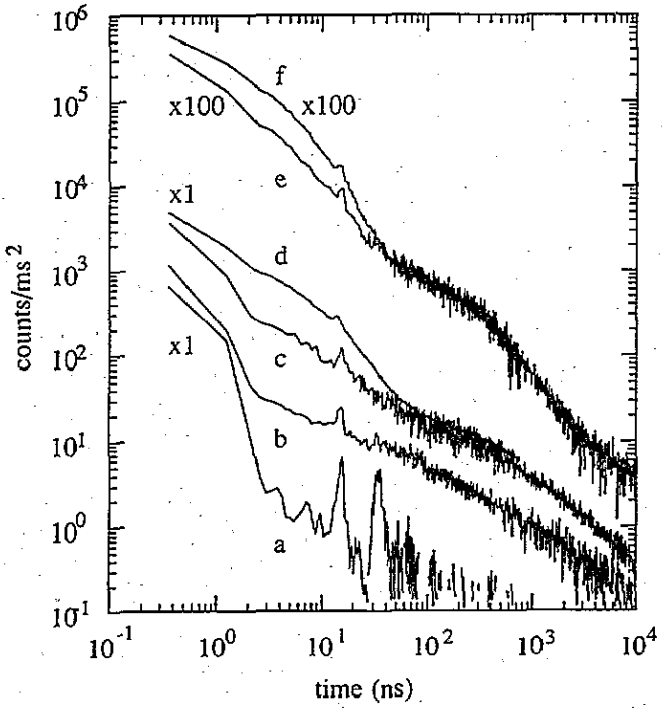

Figure 9. Gamma-ray-induced luminescence decay of LaF_3:Nd. The doping concentrations and crystal thicknesses are no crystal (curve a), 0 mol%, 5.0 mm(curve b), 3.1 mol%, 2.5 mm (curves c and d), 13.8 mol%, 2.0 mm (curves e and f). Curve d and f were measured in N_2 atmosphere; the other curves were measured in air. The curves e and f have been multiplied by 100 for clarity.

The measured decay curves are shown in figures 9–11. We note that even if no sample was mounted on the start photomultiplier (figure 9, curve a), we still obtained a non-zero readout. This is due to the detection by the stop photomultiplier of Cherenkov light emitted from the quartz window of the start photomultiplier and from the sample mounted on it. The peaks at about 15 ns and 35 ns are artificial images of the emission near time zero due to the electronics set-up.

A compilation of the results of an analysis of the decay measurements and a comparison to decay times reported in the literature is given in table 3. We will now make a few comments on this table.

(i) Cherenkov events are present in all measurements. Since the geometry and electronic set-up used was the same for all measurements, for small samples the contribution from this effect is given by figure 9, curve a. Only in the largest samples is some additional Cherenkov signal expected. Note that Cherenkov contributions are only important below 2 ns.

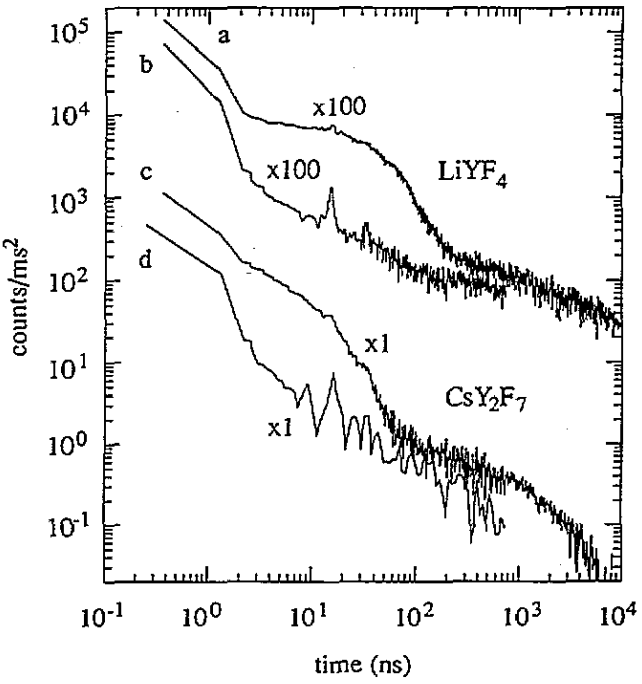

Figure 10. Gamma-ray-induced luminescence decay of 7.0 mm thick $LiYF_4$:Nd (0.9 mol%) (curves a and b) and 2.3 mm thick CsY_2F_7:Nd (3 mol%) (curves c and d). Measurements were performed in air. For curves b and d a UV filter (cut-off at 280 nm) was placed between the sample and the detector. The curves a and b have been multiplied by 100 for clarity.

(ii) LaF_3:Nd decay curves are complicated by the presence of about 0.04 mol% Ce^{3+} in the 3.1 mol% doped sample, with a decay time of 27 ns [35], and 0.004 mol% Pr^{3+}, with a decay time of 0.72 μs [12]. The concentrations were estimated from the optical absorption spectra [12, 34]. The 13.8 mol% Nd-doped crystal contains about 0.003 mol% Pr^{3+} and less than 0.004 mol% Ce^{3+}. Despite the presence of Ce and Pr emission, the shortening of the Nd^{3+} $4f^3 \rightarrow 4f^3$ decay times when increasing the Nd^{3+} concentration is evident in figure 9. This is in agreement with data from the literature.

(iii) The Nd^{3+} $4f^25d \rightarrow 4f^3$ decay time observed under optical excitation in $LiYF_4$:Nd (0.5 mol%) by Payne and Wilke [36] is shorter than the scintillation decay time we observe in the 0.9 mol% doped sample. This is indicative of a mechanism that causes Nd^{3+} excitation at later times.

(iv) The decay at < 2 ns in BaY_2F_8 is not due to Cherenkov light alone. At times $\lesssim 1$ ns, the emission of figure 11, curve a, is about a factor eight more intense than the Cherenkov emission shown by figure 9, curve a, and the BaY_2F_8 sample is so small that a Cherenkov intensity higher than that of figure 9, curve a, is unlikely. By subtracting figure 11, curve b, from curve a we obtained the emission from the BaY_2F_8:Nd (0.7 mol%) sample in the wavelength region from 180 to 280 nm. It is described by two exponentials, one with a 1/e decay time of 0.9 ± 0.1 ns, and a relatively weak one with a decay time of 16 ± 6 ns. In the $\simeq 0.04$ mol% doped sample, the 16 ns component was diminished relative to the 0.7 mol% doped sample. Therefore we assign the 0.9 ns component to CL and the 16 ns component to Nd^{3+} $4f^25d \rightarrow 4f^3$ luminescence. We did not obtain evidence for CL emission with a decay time of 3 ns, as reported by Aleksandrov *et al* [37]. Unfortunately,

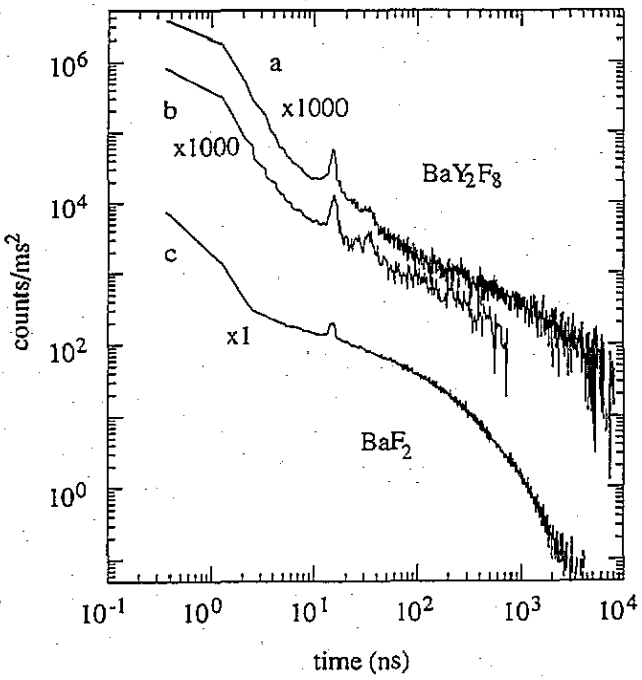

Figure 11. Gamma-ray-induced luminescence decay of 1.0 mm thick BaY_2F_8:Nd (0.7 mol%) (curves a and b) and 2.2 mm thick BaF_2:Nd (11 mol%) (curve c). Curves are measured in air. For curve b a UV filter was placed between sample and detector. The curves a and b have been multiplied by 1000 for clarity.

Table 3. Decay times of the emission observed under gamma irradiation at room temperature. A comparison is made with data from the literature for samples with about the same Nd^{3+} content.

Host	Nd concentration (mol%)	Figure	$\tau(4f^25d)$ (ns)	$\tau(^4D_{3/2})$ (μs)	$\tau(^2P_{3/2})$ (μs)	Remarks
None	—	9a	—	—	—	Cherenkov (< 2 ns)
LaF_3	0	9b	—	—	—	STE (host)
	3.1	9c,d	6.7±0.3	12 [49]	93 [49]	also Ce^{3+} ($\tau = 27$ ns), Pr^{3+} ($\tau = 0.72$ μs)
	13.8	9e,f	5.0±0.5	~0.3		also Pr^{3+}
				< 0.5	< 0.7	interpolated from [49]
$LiYF_4$	0.9	10a,b	42 ± 1	—	—	—
	~0.5	—	23	~0.8	—	[36]
	1	—	—	1.1	27	interpolated from [27]
CsY_2F_7	3	10c,d	11 ± 1	~2		—
BaY_2F_8	0.7	11a,b	16 ± 6	—	—	also CL (0.9 ns)
BaF_2	11	11c	—	—	—	CL (0.9 ns), quenched STE

our higher doped BaY_2F_8:Nd crystals did not permit decay measurements because they were very thin. In these crystals, we would expect to find only a 16 ns component in the short time range, CL emission being less important at high concentrations.

(v) As in BaY_2F_8, in BaF_2 we observed a CL component. Its decay time is 0.9 ns

[38, 39]. Beyond 2 ns, the luminescence is dominated by the non-exponentially decaying, quenched, STE luminescence. The decay looks very similar to that of lanthanum doped BaF_2 [40].

4. Discussion

In this section, we will mainly discuss the results for the absorption-corrected light yields (section 3.3), making use of the estimated Nd^{3+} quantum efficiencies (section 3.4). Where appropriate, a remark will be made about the decay times of the Nd emission.

In many crystals, we observed overlap between host emission bands and Nd absorption bands. This means that non-radiative energy transfer from the host emission centres to Nd^{3+} ions is possible. For LaF_3:Nd and BaF_2:Nd we calculated the resulting quenching of the host emission and excitation of Nd^{3+} emission as a function of the Nd concentration. These calculations are presented in section 4.1. For those cases where no overlap between host emission bands and Nd^{3+} absorption bands was observed, we tried to explain the data in terms of direct Nd^{3+} excitation during the scintillation process. This is discussed in section 4.2.

4.1. Energy transfer from host emission centres to Nd^{3+} ions

In several energy-transfer processes from host emission centres (HCs) to Nd^{3+} ions, the number $N_{HC}(t)$ of HCs host emission centres present in the crystal after their creation at time $t = 0$ is given by

$$dN_{HC}(t)/dt = -\left[1 + h(t/\tau_{HC})\right]N_{HC}(t)/\tau_{HC}. \tag{8}$$

The first term on the right-hand side describes internal radiative and non-radiative decay of the host emission centre. If $\tau_{HC,r}$ is the radiative decay time and $\tau_{HC,nr}$ is the non-radiative decay time, then we have $1/\tau_{HC} = (1/\tau_{HC,r}) + (1/\tau_{HC,nr})$. Thus, if $H(x)$ is the primitive function of $h(x)$, the time-integrated emission intensity from host emission centres is given by

$$I_{HC} = \int_0^\infty dt\, \frac{N_{HC}(t)}{\tau_{HC,r}} = \frac{\tau_{HC}}{\tau_{HC,r}} N_{HC}(0) \int_0^\infty dx\, \exp[-x - H(x)]. \tag{9}$$

The second term in (8) describes the energy transfer to accepting centres. We will assume that these are Nd^{3+} ions. In the energy transfer process, the Nd^{3+} ions will be excited into several states. Transitions from these states will take place with quantum efficiencies different for each state. Thus the time-integrated emission intensity from Nd^{3+} ions due to the energy transfer from host emission centres is the product of the amount of Nd^{3+} centres excited multiplied by an effective quantum efficiency η_{eff}:

$$I_{Nd} = \eta_{eff} \int_0^\infty dt\, h\left(\frac{t}{\tau_{HC}}\right) \frac{N_{HC}(t)}{\tau_{HC}} = \eta_{eff} N_{HC}(0) \left(1 - \int_0^\infty dx\, \exp[-x - H(x)]\right). \tag{10}$$

We note the occurrence of the same integral as in (9), which allows us to write

$$I_{Nd} = \eta_{eff}\left[N_{HC}(0) - I_{HC}\, \tau_{HC,r}/\tau_{HC}\right] \tag{11}$$

which is independent of the function $h(x)$, i.e. it is independent of the specific character of the energy-transfer process.

We will assume that the energy-transfer process proceeds via multipole–multipole interaction. Slightly generalizing equation (A15) from [41] gives

$$H(t/\tau_{HC}) = \tfrac{4}{3}\pi R_0^3 \left(\tau_{HC}/\tau_{HC,r}\right)^{3/s} \Gamma(1-3/s)\, n_{Nd} \left(t/\tau_{HC}\right)^{3/s} \tag{12}$$

where n_{Nd} is the number density of Nd^{3+} ions. $s = 6$, 8, or 10 for dipole–dipole, dipole–quadrupole, and quadrupole–quadrupole interaction respectively. R_0 is the distance at which the transfer rate $w(r) = (1/\tau_{STE,r})(R_0/r)^s$ is equal to the spontaneous radiative decay rate of the STE. For dipole–dipole interaction, R_0 is given by [42]

$$R_0^6 = \frac{3\hbar^4 c^4}{4\pi n^4} \left(\frac{\mathcal{E}}{\sqrt{\kappa}\mathcal{E}_c}\right)^4 \int_0^\infty dE\, \frac{f_{STE}(E)\, \mu_{Nd}(E)}{E^4\, n_{Nd}} \tag{13}$$

where n is the refractive index of the crystal and $\kappa \simeq n^2$ is the relative electric permittivity. $\mathcal{E}_c$ is the electric field within the crystal and $\mathcal{E}$ that at an atom in vacuum, such that both fields correspond to the same photon densities. $\mu_{Nd}(E)$ is the absorption coefficient of the Nd^{3+} ions in the crystal. $f_{STE}(E)$ is the emission spectrum of the donor centre, normalized in such a way that $\int_0^\infty dE\, f_{STE}(E) = 1$. As Dexter did [42], we will approximate $\mathcal{E}/\sqrt{\kappa}\mathcal{E}_c \simeq 1$.

For dipole–quadrupole interaction, we have

$$R_0^8 = \frac{135\alpha\hbar^6 c^6}{4\pi n^4} \left(\frac{\mathcal{E}}{\sqrt{\kappa}\mathcal{E}_c}\right)^4 \int_0^\infty dE\, \frac{f_{STE}(E)\, \mu_{Nd}(E)}{E^6\, n_{Nd}} \tag{14}$$

where $\alpha = 1.266$.

We will now investigate how well the host and Nd^{3+} emissions in LaF_3 and BaF_2 are described in terms of the above equations. (9)–(12) show that for this we have to know the parameters $\tau_{HC}/\tau_{HC,r}$, $N_{HC}(0)$ and η_{eff}, and also the parameters R_0, s and n_{Nd}, which determine the function $H(x)$. The Nd^{3+} concentration n_{Nd} was known. The other parameters are shown in table 4. The curves obtained using these parameters are shown in figures 5 and 7. Before discussing these results, we explain the parameters in table 4.

Table 4. Parameters determining the energy transfer from HCs to Nd^{3+} ions. R_0 was treated as a fitting parameter in figures 5 and 7. Calculated R_0 values are also shown.

	LaF_3		BaF_2		
	STE		CL	STE	
$\tau_{HC}/\tau_{HC,r}$	0.11		1[a]	0.48 [20]	
$N_{HC}(0)$ (MeV^{-1})	2900 ± 300		1400 [7]	(7560[b])	
η_{eff}	$\simeq 0.37$		$\leqslant 0.8$	$\leqslant 0.20$	
s	6	8	6	6	8
Experimental R_0 (Å)	11.4±0.7	10.1±0.8	7.6	8.6	8.8
Calculated R_0 (Å)	4.8	25.9	8.9	5.1	27.1

[a] Suggested by the weak temperature dependence of the CL [32, 33].
[b] From fit of BaF_2:Nd (>0 mol%) data.

4.1.1. $\tau_{HC}/\tau_{HC,r}$ and $N_{HC}(0)$. The decay rate of the STE, which has strong electron–phonon coupling, is often expressed as [43]

$$1/\tau_{STE} = 1/\tau_{STE,r} + \nu_0 \exp(-E_a/kT) \tag{15}$$

where the second term on the right-hand side is the non-radiative decay rate: ν_0 is a constant and E_a is the activation energy. In the simplest case, the quantum efficiency is equal to $\tau_{STE}/\tau_{STE,r}$. We will assume this. The STE emission intensity is then given by

$$I_{STE} = N_{STE}(0)/\left[1 + \tau_{STE,r}\,\nu_0 \exp\left(-E_a/kT\right)\right]. \tag{16}$$

For LaF_3, we obtain from fitting of the STE intensity data in figure 3(*b*) the parameters $N_{STE} = 2900 \pm 300$ MeV^{-1}, $\tau_{STE,r}\,\nu_0 = 105 \pm 10$ and $E_a = 0.065 \pm 0.006$ eV. From this and equation (15), the efficiency $\tau_{STE}/\tau_{STE,r}$ at room temperature follows (cf. table 4).

A similar analysis has been performed for the STE in BaF_2 [20]. Here $N_{STE}(0) = 16\,000$ MeV^{-1} was found. We did not obtain a good fit using this value; fitting the BaF_2:Nd data under exclusion of the 0 mol% sample yielded $N_{STE}(0) = 7560$ MeV^{-1}. CL data were obtained from the literature (cf. table 4) and result in a fair fit to the experimental data.

4.1.2. η_{eff}. The effective quantum efficiency η_{eff} of the Nd^{3+} ion was obtained from section 3.4 and table 2. Note that host STE emission spectra only have overlap with Nd^{3+} $4f^3 \rightarrow 4f^3$ absorption peaks. In the present investigation the absorption peaks near 350 nm, which lead to $^4D_{3/2}$ and $^2P_{3/2}$ excitation, are important. The quantum efficiency of the $^4D_{3/2}$ level is larger than that given in table 2, if $^2P_{3/2}$ emission which follows after non-radiative decay from the $^4D_{3/2}$ to the $^2P_{3/2}$ level is also taken into account. The efficiencies shown in table 4 are the average of this 'total' $^4D_{3/2}$ efficiency and the $^2P_{3/2}$ efficiency from table 2:

$$\eta_{eff} = \tfrac{1}{2}\left[\eta_D + (1 - \eta_D)\eta_P\right] + \tfrac{1}{2}\eta_P \tag{17}$$

where η_D and η_P are the η(300 K) entries in table 2 for the $^4D_{3/2}$ and the $^2P_{3/2}$ states, respectively. Note that equation (17) is only approximate, since in general the weighting factors for the average may be different from $\frac{1}{2}$.

The BaF_2 CL emission spectrum mainly overlaps the Nd^{3+} $4f^3 \rightarrow 4f^25d$ absorption, overlap with the $4f^3 \rightarrow 4f^3$ absorptions being small. The η_{eff} value in table 4 ($\leqslant 0.8$) pertains to the Nd^{3+} $4f^25d$ level.

4.1.3. Experimental R_0 value. Using the $\tau_{HC}/\tau_{HC,r}$, $N_{HC}(0)$ and η_{eff} values in table 4 and equations (9), (10) and (12), we fitted the experimental data for $s = 6$ and $s = 8$. The value of the fitting parameter R_0 is obtained from this (see 'experimental R_0' in table 4).

4.1.4. Calculated R_0 value. A calculation of R_0 using equations (13) and (14) was also performed ('calculated R_0' in table 4). For this we used the refractive indices $n = 1.625$ of LaF_3 at 350 nm [23], $n = 1.54$ of BaF_2 at 220 nm and $n = 1.50$ of BaF_2 at 310 nm [44]. The LaF_3 STE emission function $f_{STE}(E)$ at 300 K was obtained from the absorption-corrected STE emission (cf. section 3.3). The functions $f_{STE}(E)$ and $f_{CL}(E)$ for BaF_2 were obtained from [45]. The absorption coefficient $\mu_{Nd}(E)$ was obtained from figure 1 (after subtraction of the background) and from [13]. The same n, $f_{STE}(E)$ and $\mu_{Nd}(E)$ were used to calculate the R_0 values for $s = 6$ (equation (13)) and $s = 8$ (equation (14)). The integration was carried out over the Nd^{3+} absorption bands at wavelengths shorter than 400 nm. The neglect of the contribution to the integral for wavelengths longer than 400 nm means that the calculated R_0 values are somewhat too small (especially in LaF_3: up to $\sim 10\%$). Since it is not certain which equation ((13) or (14)) should be used (see below), we did not correct for this.

Now we will discuss the R_0 values in table 4 and compare the experimental data and theoretical curves in figures 5 and 7.

4.1.5. CL→ Nd^{3+} $4f^25d$ transfer in BaF_2. In table 4, we observe that the R_0 value calculated for the CL→Nd^{3+} $4f^25d$ energy-transfer process coincides reasonably well with the experimental value. For this energy-transfer process we assumed $s = 6$, because both the CL and the Nd^{3+} $4f^3 \rightarrow 4f^25d$ radiative emissions are dipole allowed. Also, the fit of the CL emission in figure 7 is fairly good. That the CL quenching is due to energy transfer to Nd^{3+} ions is confirmed by the absence of such large quenching in BaF_2:La [20].

A test of the theoretical Nd^{3+} $4f^25d \rightarrow 4f^3$ emission intensity is hardly possible, since only at high Nd concentrations we could separate the CL and Nd^{3+} $4f^25d \rightarrow 4f^3$ emission bands. The experimental data lie well below the theoretical curve, suggesting concentration quenching of the Nd^{3+} $4f^25d \rightarrow 4f^3$ emission, see figure 7.

4.1.6. STE→ Nd^{3+} $4f^3$ transfer in LaF_3 and BaF_2. The R_0 values calculated for energy transfer from the STE, in which the Nd^{3+} ion is excited into the higher $4f^3$ states, for $s = 6$ and $s = 8$, are respectively smaller and larger than the experimental values (cf. table 4). The STE luminescence is dipole allowed, in BaF_2 in any case (the decay time is short: 630 ns [40]). Hence the R_0 values suggest that the character of the Nd^{3+} $4f^3 \rightarrow 4f^3$ transitions is in between electric dipole and electric quadrupole character. This is plausible, since in the free ion, $4f^3 \rightarrow 4f^3$ transitions are dipole forbidden, whereas if the ion is placed in a crystal (not at a centre of inversion) even parity wavefunctions mix in, making the transitions dipole allowed [46,47].

The theoretical curves for the STE and Nd emission intensities in LaF_3 fit the experimental data only moderately well (cf. figure 5). This is ascribed to the calculated STE intensity curve: if we had used the experimental STE data in equation (11) and realizing that $N_{STE}(0) = \tau_{STE,r}/\tau_{STE}\,[I_{STE}]_{n_{Nd}=0}$, then the experimental Nd^{3+} $4f^3 \rightarrow 4f^3$ emission intensity would have been described very well up to ~ 1 mol%. At higher concentrations, our simple model fails to describe the drop in Nd^{3+} $4f^3 \rightarrow 4f^3$ emission intensity. This drop is caused by energy-transfer processes between Nd^{3+} ions, combined with non-radiative phonon-assisted decay to lower $4f^3$ states (cross relaxation). (See for instance [48] for direct evidence for such processes.) These processes cause a decrease of the emission intensity and of the effective $4f^3 \rightarrow 4f^3$ decay times τ_{eff} [49], which are proportional to each other. Indeed, the Nd^{3+} $4f^3 \rightarrow 4f^3$ intensity drop in figure 5 follows very well the decrease of the effective decay time published by Jaganath *et al* [49].

The theoretical description of the STE emission intensity in BaF_2 is reasonable for Nd concentrations larger than 0.1 mol%, but as pointed out earlier, the $N_{STE}(0)$ value used is too small (cf. table 4). This suggests that the quenching of the STE emission is not only due to Nd^{3+} $4f^3 \rightarrow 4f^3$ excitations, but also due to some other quenching process. This is confirmed by the fact that quenching of the STE emission in BaF_2:La is not much weaker than that in BaF_2:Nd. The absorption bands of La^{3+} are situated at a very high energy, and therefore have no overlap with the STE emission spectrum.

The calculated Nd^{3+} $4f^3 \rightarrow 4f^3$ emission curve in figure 7 represents an upper limit, since it is not excluded that the Nd^{3+} $4f^3 \rightarrow 4f^3$ effective quantum efficiency η_{eff} in BaF_2 is less than 0.20. Probably, the deviation from this value is not very large, considering the fact that at low Nd concentrations the calculated curve (4f in figure 7) is close to the experimental data. We note the drop in Nd^{3+} $4f^3 \rightarrow 4f^3$ emission intensity at high Nd concentrations, which is analogous to that in LaF_3.

4.2. Direct excitation of Nd^{3+} ions

In the preceding section, we did not discuss the Nd^{3+} $4f^25d \rightarrow 4f^3$ emission intensity in LaF_3. This was for the following reason. The Nd^{3+} $4f^3 \rightarrow 4f^25d$ absorption spectrum

in LaF_3 is observed for wavelengths shorter than 168 nm (cf. figure 1) and has peaks at 158.4 nm and lower [50]. Comparing this to the STE emission spectra in figure 3(*a*) suggests that overlap between the Nd^{3+} $4f^3 \rightarrow 4f^25d$ absorption and the STE emission spectra is very small. Therefore, we cannot explain the Nd^{3+} $4f^25d \rightarrow 4f^3$ emission in terms of energy transfer from the STE. Rather, we propose a different mechanism. We will consider this mechanism not only for LaF_3, but also for the other crystals investigated.

We start with a very crude estimate of the position of the energy bands in the crystal. We will neglect electronic and lattice relaxations. Consequently the results are not expected to be accurate within less than a few eV. We calculate the one electron binding energy E_b from the relation

$$E_b = E_b^{fi} + E_M \tag{18}$$

where E_b^{fi} is the binding energy of the electron on the free ion and E_M is the point charge Madelung energy at the lattice site. The electron binding energies E_b^{fi} are given by the ionization potentials of the cations and the 3.448 eV electron affinity of the F^- ion [51–53]. The Madelung energies were calculated using Ewald summation according to the method outlined in [54]. The crystal structures of LaF_3, $LiYF_4$, BaY_2F_8 and BaF_2 are found in [55]–[59]. The structure of CsY_2F_7 is not known. Therefore, calculations were done for CsF and YF_3 instead (structure: [60]). The calculated host energy bands, as well as the Nd^{3+} ground-state $4f^3\ ^4I_{9/2}$ level are shown in table 5. The bottom of the conduction band is usually situated near 0 eV. Note that the Ba^{2+} and Y^{3+} levels in BaY_2F_8 are not very different from their positions in BaF_2 and YF_3 respectively. This suggests that the Cs^+ and Y^{3+} levels in CsY_2F_7 will not be very different from their positions in CsF and YF_3 respectively. The same holds for the Nd^{3+} level.

Table 5. Estimation of the energy levels in the host materials investigated (in electronvolts). Electronic and lattice relaxations are not included.

	LaF_3	$LiYF_4$	CsF	YF_3	BaY_2F_8	BaF_2
Nd^{3+} $4f^3\ ^4I_{9/2}$	−13.2	− 6.5	—	−11.7	−12.1	−22.8[a]
						−20.2[b]
F^- $2p^6$	−14.1	− 7.4	−11.8	−13.9	−13.9	−12.9
				−14.5	−14.0	
					−14.6	
Cs^+ $5p^6$	—	—	−16.7	—	—	
Ba^{2+} $5p^6$	—	—	—	—	−18.9	−19.4
La^{3+} $5p^6$	−22.7	—	—	—	—	—
Y^{3+} $4p^6$	—	−27.9	—	−33.1	−33.5	—
Li^+ $1s^2$	—	−72.4	—	—	—	—

[a] The Nd^{3+} ion is at an O_h symmetry Ba site (no compensating F^-).
[b] Nd^{3+} at Ba site of C_{3v} symmetry (due to a charge-compensating F^- ion at the next-nearest-neighbour interstitial position).

The position of the estimated Nd^{3+} ground state level in BaF_2 is probably too low by several electronvolts. This is because in BaF_2, the Nd^{3+} ion replaces Ba^{2+}, which has a different electric charge. As a result, the BaF_2 lattice will considerably relax in the neighbourhood of the Nd^{3+} ion. The nearest neighbours, F^- ions, are attracted towards the Nd^{3+} ion, so an electron at Nd^{3+} will be less tightly bound and the Nd^{3+} levels will be located at a higher energy.

Now we consider what happens if the crystal is excited by ionizing radiation. Directly after excitation, there will be a small number of holes in deep energy levels and electrons high in the conduction band. The deep holes are soon filled by electrons from higher states, the released energy being used to create holes in the shallower energy bands and electrons in the conduction band. Auger processes replace the high-energy free electrons with a large number of low-energy electrons and holes. These processes stop as soon as the energy of the electrons and holes is no longer sufficient to create an extra free electron–hole pair. In chloride lattices, Elango *et al* found that the number of electron–hole pairs present at this stage is proportional to the energy of the absorbed high-energy photon, the mean energy needed per electron–hole pair being (1.5–2.0) E_g [61]. For a theoretical account of this see [62].

Since the band gap of the materials presently considered is about 10 eV, from the above it seems not unreasonable to make the approximation that after the relaxation processes discussed above, holes are only present in energy bands situated below the conduction band (which is at $\simeq 0$ eV) by an energy of $\simeq 20$ eV. We will assume that apart from this condition, the probability of the occurrence of a hole in an energy band is proportional to the number of electrons present in that band. This means that no efficient transfer channels between the energy bands exist. Then the number of excited Nd^{3+} ions per MeV of absorbed energy can be written

$$X_{Nd} = \left[3 n_{Nd} \Big/ \left(3 n_{Nd} + \sum_i p_i n_i \right) \right] \times 5 \times 10^4 \text{ MeV}^{-1}. \tag{19}$$

Here, n_{Nd} is again the Nd concentration; n_i is the concentration of ions giving rise to energy band i. p_i is the number of electrons in energy band i per ion. The sum runs over the energy bands with energy from 0 to -20 eV. Note that three is the number of Nd^{3+} 4f electrons per ion and that 5×10^4 is the number of electrons that can be excited per MeV of absorbed energy, assuming an average electron excitation energy of 20 eV. We will assume that direct excitation of an electron from an Nd^{3+} ion, thus leaving an Nd^{4+} ion, eventually leads to Nd^{3+} $4f^25d \rightarrow 4f^3$ emission. Then the Nd^{3+} $4f^25d \rightarrow 4f^3$ emission intensity is $I_{Nd4f^25d} = \eta_{Nd4f^25d} X_{Nd}$, where the efficiency is $\eta_{Nd4f^25d} \leqslant 0.8$ (section 3.4).

Using equation (19) and table 5, we calculated I_{Nd4f^25d} in LaF_3 assuming that $\eta_{Nd4f^25d} = 0.8$. The result is shown in figure 5, the 5d curve. For low Nd concentrations, the curve agrees with the experimentally observed values.

For pure NdF_3 however, we calculate $X_{Nd} = 7143$ MeV^{-1}, whereas the observed emission intensity is only 160 photons MeV^{-1}. This suggests that the $4f^25d \rightarrow 4f^3$ emission is concentration quenched. This is not unexpected, because there is some overlap between the Nd^{3+} $4f^25d \rightarrow 4f^3$ emission spectrum and the $4f^3 \rightarrow 4f^3$ absorption spectrum. The NdF_3 decay curve is therefore expected to be non-exponential. An approximate exponential fit would yield an effective decay time of about 6.7 ns $\times$ 160/7143 = 0.15 ns (cf. table 3). Due to the small light output of our NdF_3 samples, we were not able to detect this. However, the value is consistent with the observation of Aleksandrov *et al* [63] that the effective decay time is less than 1 ns.

For $LiYF_4$:Nd (0.9 mol%) we calculate $X_{Nd} = 56$ MeV^{-1}. For CsY_2F_7:Nd (0.3 mol%), $X_{Nd} = 19$ MeV^{-1} and for CsY_2F_7:Nd (3 mol%) $X_{Nd} = 187$ MeV^{-1} are calculated. For BaY_2F_8:Nd (0.1 mol%), $X_{Nd} = 5.6$ MeV^{-1} and for BaY_2F_8:Nd (10 mol%), $X_{Nd} = 556$ MeV^{-1} are calculated. In all cases the experimentally observed $4f^25d \rightarrow 4f^3$ intensities exceed these calculated values, although for the higher doped samples the difference is not very large: a factor of 1.3–2.5. The experimental values for the lowest-doped CsY_2F_7 and

BaY_2F_8 also exceed the calculated values, but now by a much larger factor of 15 and 30, respectively (cf. figure 6(*a*)). This is probably due to energy transfer from HCs to Nd^{3+} ions. Especially in BaY_2F_8 this is expected, because the intrinsic CL emission band extends down to 165 nm [22], whereas the Nd^{3+} $4f^3 \rightarrow 4f^25d$ absorption extends up to 185 nm.

For BaF_2:Nd (11 mol%) we find $X_{Nd} = 0$ if the Nd^{3+} ground state is really below -20 eV and 900 MeV^{-1} otherwise. Therefore, one might expect an Nd^{3+} $4f^25d \rightarrow 4f^3$ light yield of several hundred photons MeV^{-1}, which is more than observed. The reason may be the low position of the Nd^{3+} level in BaF_2. If the Nd^{3+} ground state lies below the top of the valence band, then it is energetically favourable for an Nd^{4+} ion to recapture an electron from the valence band, leaving a non-excited Nd^{3+} ion.

5. Conclusions

We investigated LaF_3, $LiYF_4$, CsY_2F_7, BaY_2F_8 and BaF_2 crystals, doped with several Nd^{3+} concentrations. The optical absorption and emission spectra show similar Nd^{3+} bands. Emissions typical of the host material (CL and STE) were also observed. From the literature and decay-time measurements, we deduced quantum efficiencies $\leqslant 0.8$ for decay from the Nd^{3+} $4f^25d$ states and between 0.1 and 1 for the decay from the Nd^{3+} $4f^3$ $^4D_{3/2}$ and $^2P_{3/2}$ states. As an exception, in BaF_2 the quantum efficiencies may be lower than these values.

Under x-ray excitation, we studied the emission intensities of the Nd^{3+} and host emission bands. In all crystals, the host emission decreased for increasing Nd concentration. The Nd^{3+} emission intensities initially increase, but at high Nd concentrations they decrease again. The maximum emission intensities we observed were, in photons MeV^{-1}:

(i) Nd^{3+} $4f^25d \rightarrow 4f^3$ emission: 500 (LaF_3), 140 ($LiYF_4$), 300 (CsY_2F_7), 700 (BaY_2F_8) and 20 (BaF_2); and

(ii) Nd^{3+} $4f^3 \rightarrow 4f^3$ emission (at $\lambda < 550$ nm): 1000 (LaF_3), 200 ($LiYF_4$, CsY_2F_7, BaY_2F_8) and 40 (BaF_2).

These values are approximate and pertain to very pure crystals (the values are absorption corrected). The maximum values were reached at Nd concentrations of $\sim$ 10 mol% and $\sim$ 1 mol% for the $4f^25d \rightarrow 4f^3$ and the $4f^3 \rightarrow 4f^3$ emissions respectively.

We have explained the emission intensities in terms of a crude energy-transfer model. In this model, the centres responsible for the host emission in the undoped crystal transfer their energy to Nd^{3+} ions, which are brought into $4f^3$ excited states (if the HC is the STE) or into $4f^25d$ states (if the host emission is CL). Apart from this, we proposed a mechanism by which Nd^{3+} ions are excited into $4f^25d$ states by subsequent hole and electron capture.

The above model does not describe the drop of the Nd^{3+} emission intensity at high concentrations, which is due to concentration quenching. Apart from this, it gives a reasonable semi-quantitative account of the experimental data. This indicates that in the crystals investigated, no unexpected efficient Nd^{3+} excitation channels exist.

Apart from emission intensities under x-irradiation, we also determined decay times of the scintillation under gamma irradiation. Nd^{3+} $4f^25d \rightarrow 4f^3$ emission decay times between 5 ns (LaF_3) and 42 ns ($LiYF_4$) were recorded.

We may now consider the usefulness of the materials investigated as scintillators. We will only consider the fast Nd^{3+} $4f^25d \rightarrow 4f^3$ emission component. In neither of the materials the intensity of this component is larger than that of the fast component of pure BaF_2 (the CL), 1400 photons MeV^{-1} [7]. Also in neither of the materials is the decay time shorter than the 0.9 ns decay time of the CL in BaF_2. Hence, one of the Nd^{3+}-doped materials

is only to be preferred instead of BaF_2 if the detecting medium is much more sensitive to the short wavelength of the Nd^{3+} emission maximum than to the CL wavelengths. This is the case if the scintillator emission is detected in a wire chamber by TMAE gas, which has 8% detection efficiency for the BaF_2 CL emission, but 31% detection efficiency for the Nd^{3+} $4f^25d \rightarrow 4f^3$ emission in LaF_3 [64]. For a CsI photocathode similar numbers are valid. As a result, combined with these detectors, under optimal conditions LaF_3:Nd ($\sim$ 10 mol%) would yield an output signal, about 1.4 times larger than if BaF_2 were used.

Acknowledgment

These investigations in the program of the Foundation for Fundamental Research on Matter (FOM) were supported by the Netherlands Technology Foundation (STW).

References

[1] Yang K H and DeLuca J A 1976 *Appl. Phys. Lett.* **29** 499
[2] Yang K H and DeLuca J A 1978 *Phys. Rev.* B **17** 4246
[3] Waynant R W 1982 *Appl. Phys.* B **26** 205
[4] Schotanus P, van Eijk C W E and Hollander R W 1988 *Nucl. Instrum. Methods Phys. Res.* A **272** 913
[5] Schotanus P, Dorenbos P, van Eijk C W E and Hollander R W 1989 *Nucl. Instrum. Methods Phys. Res.* A **284** 531
[6] Gruwé M and Tavernier S 1992 *Nucl. Instrum. Methods Phys. Res.* A **311** 301
[7] Dorenbos P, de Haas J T M, Visser R, van Eijk C W E and Hollander R W 1993 *IEEE Trans. Nucl. Sci.* at press
[8] Sakai E 1987 *IEEE Trans. Nucl. Sci.* **NS-34** 418
[9] de Mello Donega C, Ellens A, Meijerink A and Blasse G 1993 *J. Phys. Chem. Solids* **54** 293
[10] Bollinger L M and Thomas G E 1961 *Rev. Sci. Instrum.* **32** 1044
[11] Morrison C A and Leavitt R P 1982 *Handbook of the Physics and Chemistry of Rare Earths* vol 5, ed K A Gschneider Jr and L Eyring (Amsterdam: North-Holland) p 461 and references therein
[12] Elias L R, Heaps W S and Yen W M 1973 *Phys. Rev.* B **8** 4989
[13] Loh E 1968 *Phys. Rev.* **175** 533
[14] Robinson M and Cripe D M 1966 *J. Appl. Phys.* **37** 2072
[15] Chernov S P, Deviatkova L I, Ivanova O N, Kaminskii A A, Mikhailin V V, Rudnev S N and Uvarova T V 1985 *Phys. Status Solidi* a **88** K169
[16] Devyatkova K M, Ivanova O N, Oganesyan S A, Seiranyan K B and Chernov S P 1990 *Sov. Phys.–Dokl.* **35** 56
[17] Lezama A and de Araujo C B 1986 *Phys. Rev.* **34** 126
[18] Joubert M F, Jacquier B, Linarès C and Macfarlane R M 1991 *J. Lumin.* **47** 269
[19] Vakhidov Ch A, Gapparov N, Kaipov B and Tavchunskii G A 1978 *Izv. Akad. Nauk* 74
[20] Dorenbos P, Visser R, Dool R, Andriessen J and van Eijk C W E 1992 *J. Phys.: Condens. Matter* **4** 5281
[21] Brixner L H, Crawford M K, Hyatt G, Carnall W T and Blasse G 1991 *J. Electrochem. Soc.* **138** 313
[22] Jansons J L, Krumins V J, Rachko Z A and Valbis J A 1987 *Phys. Status Solidi* b **144** 835
[23] Mooney J B 1966 *Infrared Phys.* **6** 153
[24] Korczak W and Mikołajczak P 1983 *J. Cryst. Growth* **61** 601
[25] Woody C L, Levy P W and Kierstead J A 1989 *IEEE Trans. Nucl. Sci.* **NS-36** 536
[26] Sveshnikova E B, Stroganov A A and Timofeev M T 1988 *Opt. Spectrosc.* **64** 73 (Engl. Transl. *Opt. Spektrosk.* **64** 43)
[27] Jacquier B, Malinkowski M, Joubert M F and Macf.arlane R M 1990 *J. Lumin.* **45** 357
[28] Riseberg L A and Moos H W 1968 *Phys. Rev.* **174** 429
[29] Fong F K and Wassam W A 1973 *J. Chem. Phys.* **58** 956
[30] Miller M P and Wright J C 1979 *J. Chem. Phys.* **71** 324
[31] Moulton P F 1982 *CRC Handbook of Laser Science and Technology* vol 1, ed M J Weber (Boca Raton, FL: Chemical Rubber Company) p 21
[32] Schotanus P, van Eijk C W E, Hollander R W and Pijpelink J 1985 *Nucl. Instrum. Methods* A **238** 564

[33] Kubota S, Ruan(Gen) J, Itoh M, Hashimoto S and Sakuragi S 1990 *Nucl. Instrum. Methods* A **289** 253
[34] Yang K H and DeLuca J A 1977 *Appl. Phys. Lett.* **31** 594
[35] Moses W W and Derenzo S E 1990 *Nucl. Instrum. Methods Phys. Res.* A **299** 51
[36] Payne S A and Wilke G D 1991 *J. Lumin.* **50** 159
[37] Aleksandrov Yu M, Kuusmann I L, Makhov V N, Mirov S B, Uvarova T V and Yakimenko M N 1991 *Nucl. Instrum. Methods Phys. Res.* A **308** 208
[38] Kubota S, Suzuki M, Ruan(Gen) J, Shiraishi F and Takami Y 1986 *Nucl. Instrum. Methods Phys. Res.* A **242** 291
[39] Visser R, Dorenbos P, van Eijk C W E and den Hartog H W 1992 *J. Phys.: Condens. Matter* 4 8801
[40] Visser R, Dorenbos P, van Eijk C W E and den Hartog H W 1992 *J. Phys.: Condens. Matter* 4 8801
[41] Inokuti M and Hirayama F 1965 *J. Chem. Phys.* 43 1978
[42] Dexter D L 1953 *J. Chem. Phys.* **21** 836
[43] Williams R T and Song K S 1990 *J. Phys. Chem. Solids* **51** 679
[44] Schotanus P, Stam G, Gerritse E, Utts B and Briaux B 1992 *Scintillation Detectors* (Nemours: Harshaw-QS)
[45] Visser R, Dorenbos P, van Eijk C W E, Meijerink A, Blasse G and den Hartog H W 1993 *J. Phys.: Condens. Matter* **5** 1659
[46] Judd B R 1962 *Phys. Rev.* **127** 750
[47] Ofelt G S 1962 *J. Chem. Phys.* **37** 511
[48] Buisson R and Liu J Q 1984 *J. Physique* **45** 1523
[49] Jaganath H, Basu S K and Venkateswarlu P 1979 *Chem. Phys. Lett.* **66** 313
[50] Heaps W S, Elias L R and Yen W M 1976 *Phys. Rev.* **13** 94
[51] Weast R C and Astle M J (ed) 1979 *CRC Handbook of Chemistry and Physics* (Boca Raton, FL: Chemical Rubber Company)
[52] Martin W C, Zalubas R and Hogan L 1978 *Atomic Energy Levels—the Rare Earth Elements* NSDRS-NBS60 (US Department of Commerce, National Bureau of Standards)
[53] Samsonov G V (ed) 1968 *Handbook of Physicochemical Properties of the Elements* (New York: IFI/Plenum)
[54] van Gool W and Piken A G 1969 *J. Mater. Sci.* 4 95 and references therein
[55] Zalkin A, Templeton D H, Hopkins T E, 1966 *Inorg. Chem.* 1466
[56] Keller C and Schmutz H 1965 *J. Inorg. Nucl. Chem.* **27** 900
[57] Thoma R E, Wearer C F, Friedman H A, Insley H, Harris L A and Yakel Jr H A 1961 *J. Phys. Chem.* **65** 1096
[58] Izotova O E and Aleksandrov V B 1970 *Dokl. Akad. Nauk* **192** 1037 (Engl. Transl. *Sov. Phys.–Dokl.* **15** 525)
[59] Landolt–Börnstein 1993 *New Series* Group III, vol 7(a–h), ed K H Hellwege and A M Hellwege (Berlin: Springer)
[60] Wyckoff R W G 1963 *Crystal Structures* vols 1, 2 (New York: Wiley)
[61] Elango M, Kikas A, Nõmmiste E, Pruulmann J and Saar A 1982 *Phys. Status Solidi* b **114** 487
[62] Kikas A and Elango M 1985 *Phys. Status Solidi* b **130** 211
[63] Aleksandrov Yu M, Makhov V N, Uvarova T V and Yakimenko M N 1990 *Sov. Phys.–Lebedev Inst. Rep.* No 6 46
[64] Visser R, Dorenbos P and van Eijk C W E 1993 *Heavy Scintillators for Scientific and Industrial Applications; Proc. 'CRYSTAL 2000' Int. Workshop* ed F De Notaristefani, P Lecoq and M Schneegans (Gif-sur-Yvette: Editions Frontières) pp 421–5